Nuclear Instruments and Methods in Physics Research A 700 (2013) 91–98

Contents lists available at SciVerse ScienceDirect

Nuclear Instruments and Methods in Physics Research A

journal homepage: www.elsevier.com/locate/nima

A proposed fiber-optic neutron monitor

Jonathan D. Weiss *

JSA Photonics LLC, P.O. Box 2930, Corrales, NM 87048, USA

ARTICLE INFO

Article history:
Received 10 April 2012
Received in revised form
8 August 2012
Accepted 14 October 2012
Available online 23 October 2012

Keywords:
Neutron monitor
Fiber-optic sensor
Interferometry
Nuclear isotopes

ABSTRACT

An interferometric fiber-optic sensor is proposed as a neutron detector. The basic mechanism is the absorption of neutrons by the constituent atoms of the fiber: silicon, germanium, and oxygen. As a result, the isotopic mass of these elements increases and thereby decreases certain infrared vibrational frequencies. These changes impact the refractive index of the core and cladding of the fiber and therefore the propagation constant of the fundamental mode of the singlemode fibers constitutes the interferometer. This neutron-induced shift in the propagation constant produces a corresponding shift in the phase of the light emerging from one fiber of a Mach–Zehnder interferometer. A review of the basics of singlemode fibers is presented, and the changes in indexes and the propagation constant are calculated under varying shifts in isotopic mass. Reference is made to the computational tool available for a simulated sensor response. Some neutron absorption cross-sections as functions of neutron kinetic energy are presented, along with a possible design of the sensor.

1. Introduction

Neutron monitoring is important in many areas, such as health physics and radiation safety [1], cascading effects in the study of cosmic radiation [2], for monitoring of the performance of nuclear power plants [3], and for the monitoring of special nuclear materials for homeland security [4]. An extensive review of neutron detection techniques is presented in Ref. [5], with no mention of any fiber-optic methods, although plastic scintillating optical fibers are manufactured by Saint-Gobain [6]. The capture efficiency of the light generated in their interior is, however, only a few percent; most of it escapes out the sides, rather than be guided to either end. Also not mentioned in Ref. [5] is the increasing use of the wide-bandgap semiconductor material, silicon carbide, as a neutron detector. As discussed in Ref. [7], such a detector is in the form of a reversed-biased p–n junction created by a thin, lightly doped layer of SiC in contact with a thick, heavily doped layer of the same material. The dopant is nitrogen. A lithium converter is placed in front of the device which converts neutrons to He^3 and He^4. These nuclei produce ionization in the form electron-hole pairs within the SiC, which, in turn, generate a current pulse that comprises the signal. The advantage of SiC over similar devices based on silicon is its greater ability to withstand high radiation-induced damage and a higher-temperature capability.

In this paper, a proposal for an interferometric fiber-optic neutron monitor is presented, which is an outgrowth of the proposal presented in Ref. [4]. Since it is interferometric, high sensitivity is expected. In addition, the standard advantages of optical fibers apply: EMI immunity, intrinsic safety, and geometric flexibility. Furthermore, this approach allows the effects of gamma radiation to be separated from those of neutrons; in fact, the two can compliment each other. Many such interferometers measure environmental factors such as temperature and pressure by means of the changes in refractive index and length that they induce in the fiber. In this case, the means is the change in refractive index induced by neutron absorption. This change occurs by means of the reduction in vibrational frequencies caused by the increase in the isotopic mass of the various atomic nuclei that constitute the glass. It will be quantified later through the use of the Sellmeier and mixed-Sellmeier expressions for the refractive index. Before discussing the details, we present certain relevant facts about singlemode optical fibers and such interferometric sensors.

2. Singlemode optical fibers

2.1. Material and geometric characteristics

Since the proposed fiber-optic sensor is interferometric, the fibers of which it is made are singlemode. Otherwise, the interference pattern which is supposed to produce will be washed out. (An exception might be a self-interfering sensor in which a very few modes of a given few-mode fiber interfere among themselves

* Tel.: +1 505 821 8256; fax: +1 505 792 8563.
E-mail address: jondweiss@aol.com

0168-9002/$ - see front matter © 2012 Elsevier B.V. All rights reserved.
http://dx.doi.org/10.1016/j.nima.2012.10.045

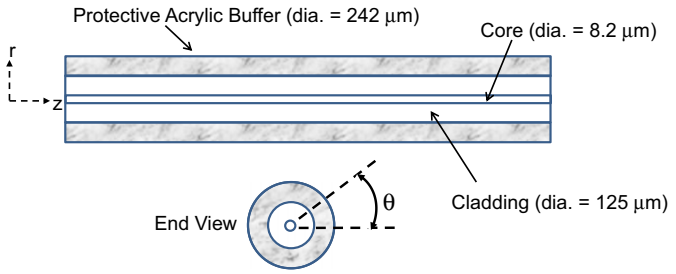

Fig. 1. Singlemode optical fiber: side and end views of a typical singlemode optical fiber (manufactured by Corning).

to produce an interference pattern at its output facer. This is in contrast to the interference pattern produced by combining outputs from separate singlemode fibers, as will be later described.) The singlemode fiber under consideration is a standard telecommunications fiber from Corning, known as "SMF-28e+" [8]. The use of a standard fiber, without modification, is an advantage of this sensor. The fiber is illustrated in Fig. 1.

The fiber consists of a core having a diameter of 8.2 μm and a refractive index=1.4536 at a vacuum wavelength (λ_o) of 1310 nm (1.31 μm), for which laser diode sources are readily available. It consists of silica with 4.71% of the silicon atoms replaced by germanium atoms. The germanium occupies the same position of silicon after replacing it, namely in the center of a tetrahedron formed by four oxygen atoms. The core is surrounded by a cladding, having a diameter of 125 μm, consisting of pure silica and having a refractive index=1.4468 at the same wavelength. This wavelength has been chosen for our discussion because the Corning datasheet [8] lists certain wavelength-dependent characteristics at 1319 nm (presumably because it is the wavelength of zero material dispersion in pure silica). The refractive indexes and the percent germanium were deduced from those characteristics and a method of calculating the refractive index is to be discussed shortly. The glass fiber is surrounded by an acrylic buffer that protects it from the environment. Its nominal diameter is 242 μm.

2.2. Functional characteristics

A mode of an optical fiber is a characteristic pattern of electric and magnetic fields that vary in a certain manner with r and θ in any transverse plane, but which propagate in the z direction. For fibers with a small index difference between the core and the cladding, such as this one, the fields are essentially perpendicular to the fiber axis. Aside from a time dependence of $\exp(-i\omega t)$, the electric or magnetic fields can be written as some combination of [[9], p. 287]:

$$[F_l(r)\cos l\theta]\ \exp(i\beta_l z)\ \text{ and }[F_l(r)\sin l\theta]\ \exp(i\beta_l z) \tag{1}$$

In these expressions, the subscript l designates the mode number and β_l designates the associated propagation constant. Differences in the phase factor, $\beta_l z$, lead to the interference of signals from two different fibers. When only the fundamental mode, with $l=0$, can propagate, we have singlemode operation and a potentially clean interference pattern. This state of affairs will be assumed in the discussion of the proposed sensor, with the condition for it to occur presented below.

An important characteristic of optical fibers is their numerical aperture, or *NA*. The *NA* is defined as

$$NA = \sqrt{n_{co}^2 - n_{cl}^2} \tag{2}$$

where n_{co} and n_{cl} are the core and cladding refractive indexes, respectively. The numerical aperture is the sine of the largest angle that an incoming light ray can make with the fiber axis and still be guided by total internal reflection. We can only interpret the *NA* in this manner when geometrical optics provides an adequate description of light propagation within the fiber. In the case of singlemode operation, the optical wavelength is long enough compared to the core diameter that such a description is no longer possible, but the *NA* remains an useful parameter. For example, Corning lists the *NA* of this fiber as 0.14. This number made it possible to deduce the core index, when the cladding index was known.

Another important characteristic of an optical fiber is its *V*-number (*V*), defined as

$$V = \left(\frac{\pi D}{\lambda_o}\right) NA \tag{3}$$

where D is the core diameter. It is well-established theoretically [10, p. 302] that a circular, step-index fiber supports only a single guided mode (the "fundamental") when $V<2.405$ (or, more properly, two guided modes that have the same propagation constant and field distribution, but only differ in their polarization). Additional guided modes come into existence for values of $V>2.405$, although the number of guided modes does not change continuously with V. In the case of a typical multimode fiber having a core diameter of 100 μm and a $NA=0.2$, $V=54.4$ and the number of guided modes can be shown to be 1972 for a wavelength of 1000 nm [10, p. 470].

These last few comments make it clear that the term, "singlemode optical fiber", is a slight misnomer, since any particular optical fiber (having a fixed *NA* and *D*) can be multimode or singlemode, depending on the wavelength of the light being guided by it. For example the Corning fiber is multimode for a wavelength below 1260 nm. This is known as the "cutoff wavelength" and it is called out in the Corning datasheet as such. However, for it to be as multimode as the typical fiber just mentioned, the wavelength would have to be about 55 nm, which is well below any wavelength where the fiber can transmit over useful distances. This estimate ignores any wavelength dependence of the refractive index. Similarly, the typical multimode fiber just mentioned would be singlemode for a wavelength of 22,000 nm, which is well above any wavelength where the fiber can transmit over useful distances. Thus, a singlemode fiber can be considered as such if it exhibits singlemode operation over a range of wavelengths where useful transmission occurs.

The reader may have noticed an inconsistency between a *V*-number of 2.405 and a cutoff wavelength of 1260 nm. Given the stated values of the *NA* and *D*, a wavelength of 1500 nm is the calculated cutoff, while 1260 nm results in a *V*-number of 2.862. This value of the *V*-number places the fiber within the four-distinct-mode regime, not at the entrance of it [10, p.302]. (That regime, in fact, exists for $2.405<V<3.832$, where three additional modes are guided by the fiber [11, p. 13].) However, as pointed out in a Corning technical note [12], the cutoff wavelength obtained from a *V*-number of 2.405 applies to a relatively unperturbed, uncabled fiber. In standard telecommunications use, a fiber is cabled for its own protection. Depending on the nature of the cabling, microbends can be induced in the fiber, which can cause light to be scattered out of it, rendering such light undetectable at the end of a long enough length of fiber. This is particularly true of the so called higher-order, less-well-confined modes than the fundamental. Thus, only the fundamental survives practical transmission distances, when, according to Corning, the wavelength is greater than 1260 nm. Whether that will be true in this sensor application or whether a wavelength greater than 1500 nm will be required, will depend on the details of deployment that are not now available. If the former is true, then the self-interference mentioned earlier would not be viable because

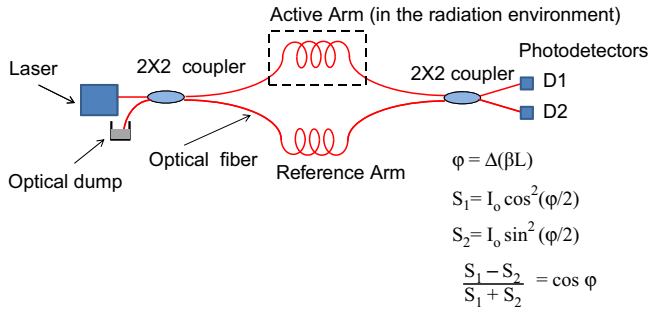

Fig. 2. Fiber-optic interferometer using a Mach–Zehnder configuration: S_1 and S_2 are the signals from the photodetectors D_1 and D_2, respectively. The angle φ is the phase difference between the light emerging from the active and reference arms of the interferometer.

only one mode would survive to the output face of the sensor. For our current purpose, we assume singlemode operation at a wavelength of 1310 nm.

2.3. The propagation constant

The parameter, β, in Eq. (1) is known as the propagation constant. As stated above, differences in the phase factor, βL, where L is the fiber length, lead to an interference pattern. Such an interference pattern can be (and has often been) produced by the Mach–Zehnder configuration shown in Fig. 2. It would be desirable for the coherence length of the light source to be greater than the length of the fibers in the arms of the interferometers. The 2×2 couplers act like 50/50 bulk-optics beam splitters, with one leg of one coupler dead ended into a medium that prevents any unwanted reflections. The interference pattern is not displayed on a screen, but in the phase-dependent outputs of the two photodetectors. We note that the sum of the two outputs is a constant because energy is conserved, and that processing the two signals, as shown in the figure, eliminates the effect of signal fluctuations in the source.

It is well-established theoretically that, for any guided mode, $(2\pi n_{\mathrm{clad}}/\lambda_o)<\beta<(2\pi n_{\mathrm{core}}/\lambda_o)$ [10, chap. 8], where n_{clad} and n_{core} are the refractive indexes of the clad and core, respectively. The lower limit corresponds to cutoff for a particular mode, when its field extends a great distance into the cladding. The upper limit is approached when the mode becomes extremely well guided, in which case its field extends a negligible distance into the cladding.

For the fiber under consideration here, the fractional difference between these two limits is only about 0.0047, which is negligible for many purposes. However, interferometrically, it is not. $(L/\lambda_o)(n_{\mathrm{core}}-n_{\mathrm{clad}})=1$ for $L\approx 0.2$ mm. In other words, the difference between these two values of β produces a phase difference of 2π in a tiny length of fiber. It produces a phase difference of 5000 times that amount in a mere 1 m length of fiber. Thus, very small changes in the propagation constant can produce significant changes in the outputs of the photodetectors in Fig. 2.

2.4. Approximate formulas for the propagation constant

The propagation constant is the eigenvalue of a complex eigenvalue problem defined by Maxwell's equations and the boundary conditions at the core-cladding interface of a round dielectric waveguide, better known as an optical fiber [10]. Obviously, given the cylindrical geometry, Bessel functions of various "flavors" are involved. Although the problem can be, and has been, solved numerically for the propagation constant, various convenient analytic approximations have been proposed,

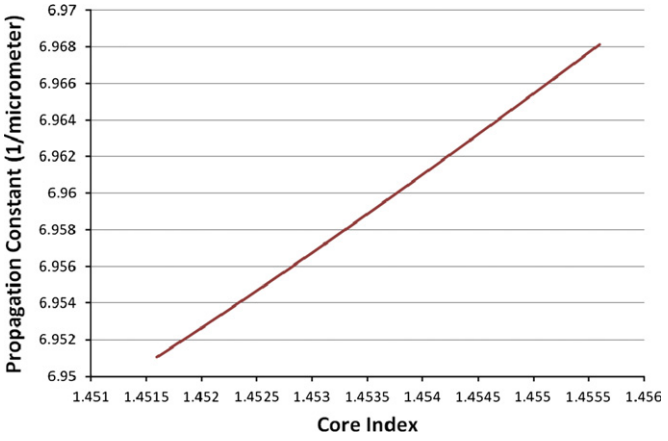

Fig. 3. The propagation constant of the fundamental mode vs. the core index, for a fixed cladding index of 1.4468.

as noted in Ref. [13]. As also noted in this reference, the most accurate of these is contained in Ref. [14]. Because of its accuracy and simplicity, it will be used for our current purpose. That purpose is to determine the change in propagation constant as a result of a change in either or both refractive indexes. In this case, the change would be caused by neutron absorption, to be discussed later, and lead to a phase shift in one arm of a fiber-optic interferometer.

The discussion of the approximation is more accessible from Ref. [11, chap. 1] than from Ref. [14], where it can be easily inferred that

$$\beta^2 \approx \left(\frac{1}{a^2}\right)\left[kan_{\mathrm{clad}}+(1.1428\,V-0.9960)^2\right] \tag{4}$$

where k is the propagation constant of light in a vacuum and a is the radius of the fiber core.

Figs. 3 and 4 show the calculated propagation constant using Eq. (4). In Fig. 3, the cladding index is fixed at the Corning value of 1.4468 and the core index varies between 1.4516 and 1.4536, which is the core value of the Corning fiber, 1.4536 ± 0.002. In Fig. 4, the core index is fixed at 1.4536 and the cladding value varies between 1.4448 and 1.4488, or 1.4468 ± 0.002. Over this range of refractive indexes, the difference between the "exact" numerical value for β and that predicted by Eq. (4) is in the fourth or fifth decimal place.

3. The calculation of refractive index

Based on the discussion immediately above, it is obvious that the calculation of refractive index is necessary before proceeding with a determination of the variation in the propagation constant, as in Figs. 3 and 4. Probably the most widely used formula for this purpose is the ubiquitous three-term Sellmeier equation, mentioned in countless sources, including Ref. [10]. It is

$$n^2=1+\sum_{i=1}^{3}A_i\frac{\lambda^2}{\lambda^2-\lambda_i^2} \tag{5}$$

where the index i denotes the i^{th} optical transition, A_i is the dimensionless strength of that transition (proportional to the probability that it will occur), λ_i is the resonant wavelength of that transition, and λ is the vacuum wavelength of the light passing through the material. Clearly, the equation is invalid near a resonance, where it predicts an index that can be arbitrarily large in magnitude and of either sign. For the glassy materials of optical fibers, the divergence near a resonance is no restriction on the use of this equation where they transmit well, which is in the

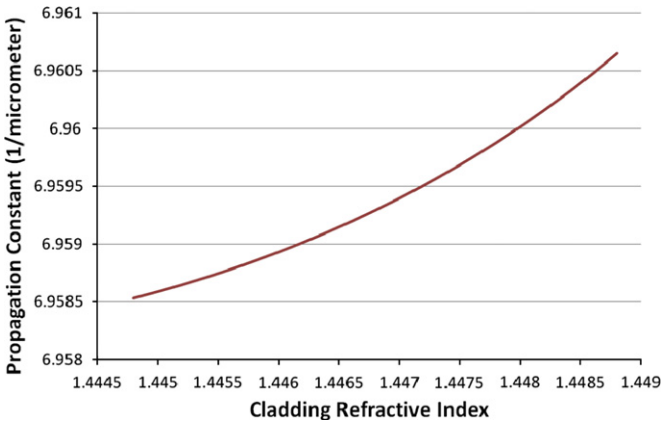

Fig. 4. The propagation constant vs. the cladding index for a fixed core index of 1.4536.

visible and near infrared. Two of the resonant wavelengths appearing in the equation are in the ultraviolet and one is in the mid-infrared.

For a composite glass, such as the germano-silicate glass that makes up the core, it is possible to obtain a good fit using Eq. (5) [15], but a generalization of Eq. (5), known as the mixed Sellmeier equation, is more appropriate for our purpose [16]. This equation combines the Sellmeier coefficients, A_i and λ_i, from each of the pure glasses, SiO_2 and GeO_2 according to their mole fraction in the composite. The result is

$$n^2 = 1 + \sum_{i=1}^{3} [A_{is} + X(A_{iG} - A_{is})] \frac{\lambda^2}{\lambda^2 - [\lambda_{iS} + X(\lambda_{iG} - \lambda_{is})]^2} \tag{6}$$

where X is the mole fraction of GeO_2, A_{iG} and A_{iS} are the strengths of the i^{th} transition in pure GeO_2 and SiO_2, respectively, and λ_{iG} and λ_{iG} are the resonant wavelengths of those transitions in those materials. For convenience, the required coefficients are listed in the table below, as obtained from Ref. [16]. We note that the two pure glasses have the same structure, with either Ge or Si contained within a tetrahedron of four oxygen atoms, one at each corner.

Normally, the Sellmeier fit to the experimental data is used to determine the refractive index at various wavelengths within its wavelength range of validity. Here, in contrast, we are fixing the wavelength and examining its behavior with changes in λ_i. The table indicates that, as stated previously, two of the three resonant wavelengths are deep in the UV and one is in the mid IR. Since the first two result from electronic transitions, they are independent (to an excellent approximation) of the mass of the nuclei. The one in the IR is vibrational in nature and therefore does depend on the nuclear mass. Thus, it is this wavelength that is of concern to us.

4. Relevant molecular vibrations

The relevant molecular vibrations for either GeO_2 or SiO_2 appear to be those presented in Ref. [17, Fig. 3.11]. Only those for SiO_2 are actually presented, but because of the similarity in structure between the two glasses, it is assumed that these are the same for GeO_2. These are characterized as asymmetric bending or asymmetric stretching involving two silicon or germanium atoms and one oxygen atom, as shown in Fig. 5. From Ref. [17] the estimated resonant wavelengths associated with these modes are 9.43 μm and 8.40 μm, respectively, for SiO_2. Their average is 8.92 μm, which is reasonably close to the experimentally determined value of ~9.90 μm, as shown in the table. It is for this reason that these modes are being considered. It can be readily

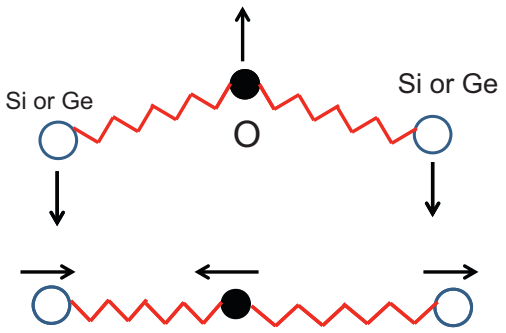

Fig. 5. Pictorial representation of the relevant vibrational modes of SiO_2 or GeO_2 in the glass matrix of an optical fiber.

shown from simple harmonic oscillator theory that f, the frequency of these modes is of the form

$$f = \sqrt{\frac{k}{M_r}} \tag{7}$$

where k acts as a spring constant and M_r is a reduced mass. The reduced mass is

$$\frac{1}{M_r} = \frac{2}{M_O} + \frac{1}{M_{Si,\ Ge}} \tag{8}$$

where M_O is the mass of the oxygen nucleus and $M_{Si,Ge}$ is the mass of either the silicon or germanium nucleus. This expression can be made intuitively obvious by allowing either mass to approach infinity. The effective (estimated) spring constants can be adjusted so that the average wavelength is the experimental λ_{3S} or λ_{3G}. Then one can readily show that

$$\lambda' = \lambda \sqrt{\frac{M_r'}{M_r}} \tag{9}$$

where λ refers to the experimental λ_{3S} or λ_{3G} and the primed quantities refer to values resulting from changes in nuclear mass.

5. Isotopic distribution of elements Ge, Si, and O

Before examining the effects on neutron absorption on the refractive index, let us present the "natural" isotopic distribution of the elements germanium, silicon, and oxygen. These are shown in the table below, obtained from Ref. [18], and references contained therein, along with the weighted average of the atomic mass numbers. These weighted averages are, presumably, what appears in the fiber before neutron irradiation. (The effect of variations in nuclear binding energy is small and is being ignored in this treatment.)

6. Effect of the shift in the isotopic masses

Let us first look at the consequences of the shift in isotopic mass distribution, without regard to the nature of the neutron irradiation that causes it or the neutron absorption cross-sections. We will do so by first computing the change in refractive index of the core and cladding by using Table 1 and Eqs. (8), (9), (5), and (6), while allowing the atomic weight of each the three elements to vary between the weighted average and the maximum possible, in various combinations. For germanium, this range is from 72.67 to 76; for silicon, it is from 28.30 to 30; and for oxygen, it is from 16.00 to 18.00. Then Eq. (4) will be used to calculate the change in propagation constant for the various combinations. Doing so will quantify the response of the sensor under the most

Table 1
Parameters used in the mixed Sellmeier equation, Eq. (6).

SiO_2 (0.21 μm < λ < 3.71 μm)		GeO_2 (0.37 μm < λ < 4.28 μm)	
A_{1S}	0.6961663	A_{1G}	0.80686642
A_{2S}	0.4079426	A_{2G}	0.71815848
A_{3S}	0.8974794	A_{3G}	0.85416831
λ_{1S} (μm)	0.0684043	λ_{1G} (μm)	0.068972606
λ_{2S} (μm)	0.1162414	λ_{2G} (μm)	0.15396605
λ_{3S} (μm)	9.896161	λ_{3G} (μm)	11.841931

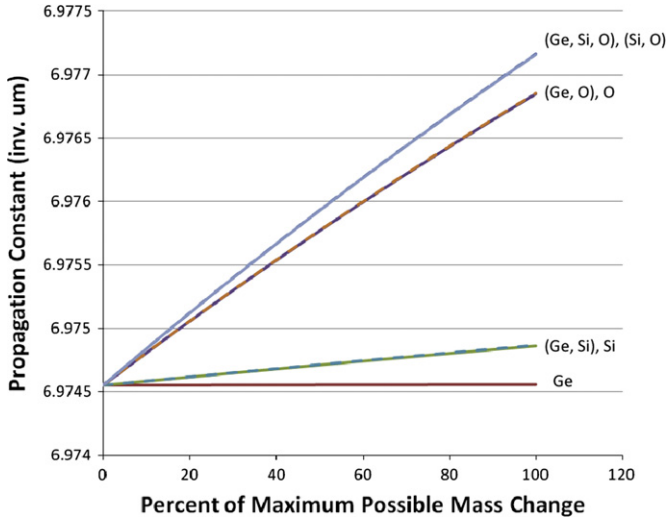

Fig. 6. The propagation constant vs. the percent of maximum mass change for various combinations of Si, Ge, and O. Each of the elements is assumed to undergo the same percent mass change in every case. The effect of changes in Ge is negligible on this scale, but still produces an interferometric signal.

pessimistic assumption, producing zero response, to the most optimistic possible.

Fig. 6 illustrates how the propagation constant changes when the various combinations of the three nuclei, Ge, Si, and O, increase in atomic weight from their "natural value" to their maximum possible value resulting from neutron irradiation. The abscissa is the percentage difference between these two extremes, assumed, for simplicity, to be common to all changing masses. As indicated in the legend, either all three masses change, two of the three change, or one of the three changes. It is clear from the figure that the change in the isotopic mass of germanium produces an increase in the propagation (of about 6×10^{-6}) that is not visible on the scale of the graph. However, even in this case, the change in propagation constant produces a shift in the interference pattern of one cycle in only about 1 m of fiber. Nevertheless, as a result, three other pairs of curves are indistinguishable on the same scale. The maximum possible increase in propagation constant, 0.00261/μm, produces a shift of over 2400 cycles in that same meter of fiber. A kilometer of fiber, which is not cumbersome, would produce a shift one thousand times that size. These idealized results encourage one to believe that reasonable signals can be obtained even when the nature and absorption of the neutron irradiation are explicitly considered Table 2.

7. Generation of unstable isotopes

What have not been considered in this idealized treatment are the unstable isotopes of germanium, silicon, and oxygen generated by neutron absorption and the subsequent decay chains. These processes are represented below, along with the half-lives of the unstable nuclei. They were obtained from references similar to Ref. [18].

$^{70}\mathrm{G}\,e+n\rightarrow{}^{71}\mathrm{Ge}\xrightarrow{11.4\mathrm{d}}{}^{71}\mathrm{Ga}$ (stable)

$^{74}\mathrm{Ge}+n\rightarrow{}^{75}\mathrm{Ge}\xrightarrow{82.8\mathrm{m}}{}^{75}\mathrm{As}$ (stable)

$^{76}\mathrm{Ge}+n\rightarrow{}^{77}\mathrm{Ge}\xrightarrow{11.3\mathrm{h}}{}^{77}\mathrm{As}\xrightarrow{38.8\mathrm{h}}{}^{77}\mathrm{Se}$ (stable)

$^{30}\mathrm{Si}+n\rightarrow{}^{31}\mathrm{Si}\xrightarrow{157\mathrm{m}}{}^{31}\mathrm{P}$ (stable)

$^{18}\mathrm{O}+n\rightarrow{}^{19}\mathrm{O}\xrightarrow{26.5\mathrm{s}}{}^{19}\mathrm{F}$ (stable)

These decay chains can be considered first-order, in that they involve the absorption of only one neutron. If additional neutrons are absorbed, then they can be extended, such that ^{77}Se, for example, could become the stable isotope ^{78}Se. Or they could become branched, such that ^{77}As, for example, might become ^{78}As and then ^{78}Se. The second and higher-order decay chains appear to be progressively less probable than the first, as they require the absorption of progressively more neutrons. They also require progressively more time for completion.

The effect of these processes is to change the vibrational frequencies of the original molecule through a change in electronic binding with, say, a stable isotope of oxygen. (The mass change is completely negligible.) The result will be a small change in refractive index, which adds to or detracts from the measurement of phase. Unfortunately, it may also scatter light out of the core of the fiber, reducing the amplitude of the signal. If the measurement time is small compared to the half-lives of the unstable nuclei, these processes may be unimportant. All of them require hours to days, except for the last, which requires only 26.5 s. However, so little ^{18}O occurs naturally that this process may still be inconsequential.

A post-irradiation measurement, during which all unstable isotopes eventually decay away, would provide information on the importance of the totality of these processes.

8. Thermal variations

The high sensitivity of interferometric sensors can be a curse as well as a blessing. If the temperature of the reference arm and active arm in Fig. 2 is not the same, despite one's best efforts to maintain them at the same temperature, then thermal variations will produce an unwanted signal. This signal results from the phase shift produced by the temperature dependence of both the length of the fiber and the propagation constant. Such a signal can be minimized by packaging the sensor with a large enough thermal mass that the magnitude and frequency of the temperature variations are small. If the frequency range of this unwanted signal is much lower than that of the desired signal, then the two can be separated in the signal processing. In addition, the sensor should be packaged to thermally isolate the components from ambient temperature fluctuations and to maintain the two arms as close as possible in temperature. Various techniques to deal with this problem are discussed in Ref. [19]. If the radiation itself produces a rise in temperature of the active arm, then it can be considered part of the signal, superimposed on that due to shifts in the isotopic masses. The two effects can be separated by isolating the sensor from the radiation; what is left is the permanent change produced by those shifts in mass (once any unstable isotopes have decayed away).

It may be possible to examine the thermal effects of the ambient environment on the sensor output by observing the signal in that environment, but shielded from neutron irradiation. The mechanical and thermal design, as well as the positioning and orientation, of the sensor should be such as to minimize this

Table 2
(Stable isotopes).

Germanium		Silicon		Oxygen	
Atomic mass number	Percent abundance	Atomic mass number	Percent abundance	Atomic mass number	Percent abundance
70	21.23	28	92.3	16	99.6
72	27.66	29	4.67	17	0.039
73	7.73	30	3.1	18	0.201
74	35.94				
76	7.44				
Weighted average	72.67	Weighted average	28.30	Weighted average	16.00

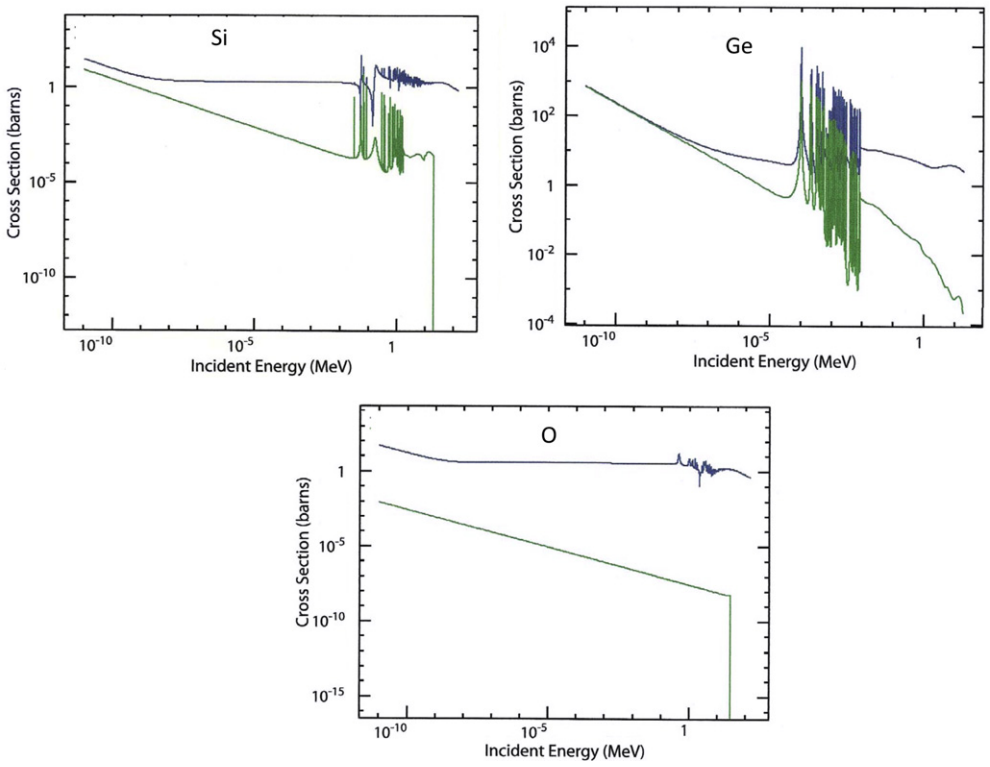

Fig. 7. Neutron absorption cross-sections vs. neutron kinetic energy (lower curves) for Ge, Si, and O. The upper curves include neutron scattering, along with absorption. (For interpretation of the references to color in this figure caption, the reader is referred to the web version of this article.)

extraneous signal. Since some neutron-sensing environments are more benign than others, the design and viability of the sensor is expected to be highly dependent on the application.

9. Neutron irradiation

Prior to any experimentation testing the response of this proposed sensor to neutron irradiation, it would be advisable to perform calculations simulating various scenarios under which it might be used. These scenarios would incorporate the neutron flux and energy distribution, the energy-dependent absorption cross-sections, and the geometry of the sensor and of the neutron source. Being made of optical fibers, the sensor geometry can be readily varied, as stated in the introduction. At least one code exists for this purpose, and that is the Monte Carlo N-Particle Transport Code (MCNP) created at Los Alamos National Laboratory [20]. However it seems premature at this point to pursue even the calculational approach, in the absence of an expressed interest and a definition of a particular application.

One readily available piece of information that is of interest at this point involves the neutron absorption cross-sections of germanium, silicon, and oxygen, examples of which are shown in Fig. 7. Such cross-sections are published by the National Nuclear Data Center as the Evaluated Nuclear Data File (ENDF) [21]. The green curves are the absorption cross-sections, while the blue are the total cross-sections. We note the energy dependence and the highly oscillatory resonance behavior in germanium and silicon. In addition, the absorption is, in every case, accompanied by the emission of a gamma ray. Depending on the neutron energy spectrum, it may behoove one to include a moderator in the design of the sensor to improve absorption. One possible design is shown schematically in Fig. 8, in which a cylindrically shaped neutron source is assumed. Ideally, the neutron reflector prevents any neutrons from reaching the reference arm of the Mach–Zehnder interferometer and is of high thermal conductivity to maintain the two arms as close to the same temperature as possible. High reflection of neutrons will produce multiple passes through the active arm, thereby increasing the chance for absorption. Steel is possible candidate for a good reflector.

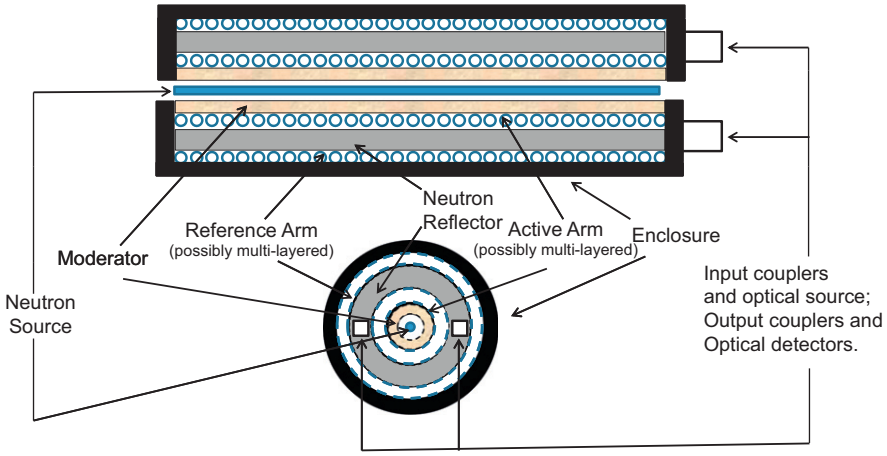

Fig. 8. Side and end views of a possible design of the neutron monitor with a cylindrical neutron source.

10. Mitigating radiation-induced darkening

In addition to generating the desired signal through changes in the isotopic mass of the constituent atoms of the fiber, neutrons and other forms of nuclear radiation impinging on the fiber can also cause damage that leads to a reduction in optical transmission. Depending on the dose, dose rate, wavelength of transmission, the nature of the fiber, etc., this "radiation-induced darkening" could be quite severe, potentially fatal to the operation of the sensor. Examples of this well-known phenomenon are shown in Ref. [4]. Even changes in isotopic mass caused by neutron absorption could result in some internally generated gamma emission, since the resulting nucleus is likely to be initially in an excited state. For example, this is the case for ^{72}Ge and ^{73}Ge [18].

Several factors can mitigate this problem. The first is that the sensor operates in the 1300–1500 nm wavelength region, as shown in Ref. [4], the effects of darkening are much less serious than at shorter wavelengths, such as the visible or very near IR. Second, optical fibers do recover from radiation-induced damage (even during exposure to radiation). It may be possible to perform the desired measurement after the sensor has been isolated from the radiation. As stated earlier, what is left after recovery is a permanent change in the fiber produced by shifts in isotopic mass. Doing this, however, will only result in a measurement of total dose.

A third mitigating factor is photobleaching, which is the reduction in radiation-induced damage caused by the presence of light within the fiber. The greater the optical power propagated through the fiber, the stronger the effect. The exact mechanism by which the defects are annealed out by light does not seem to have been offered, but the effect is well established [22–25]. In fact, a patent exists on the use of photobleaching to reduce the radiation sensitivity of a fiber-optic rotation sensor [26]. The experiments described in some of these references, particularly in Ref. [22] suggest that photobleaching is more effective in pure-silica-core fibers than those with a core doped with germanium, but Corning's singlemode fiber has a lower concentration of germanium than those multimode fibers studied in Ref. [22]. In addition, more powerful light sources exist now than at the time of the study. If having a pure-silica-core is particularly important, one could fabricate such a singlemode fiber with a fluorinated cladding. Multimode fibers with a pure-silica core and a fluorinated cladding have long existed [27] and, in fact, a singlemode specialty fiber of this type already exists [28], but for non-telecommunications use deep in the visible and near UV. The same company claims to be able to make this kind of fiber for use in the 1300 nm regime. Aside from being more "photobleachable", pure-silica-core fibers are also known to be significantly less radiation sensitive to begin with than those with a doped core. The nature of the application will determine whether a pure-silica-core fiber will be required for neutron monitoring.

A fourth mitigating factor would be the use of a separate wavelength to induce photobleaching from the one used to carry the signal. Even though, say, 1300 nm can produce photobleaching, shorter wavelengths with their higher photon energy are more effective at doing so [24,25]. A photobleaching wavelength of 835 nm was used in Ref. [24] and one of 633 nm was used in Ref. [25]. Thus, one can send photobleaching light into the neutron monitor, preferably from both ends, along with the signal wavelength, on a non-interfering basis. A single-ended photobleaching light source is used in Ref. [26].

11. Summary

A proposal for an interferometric fiber-optic neutron monitor has been presented, based on the absorption of neutrons by the nuclei making up the core and cladding of the singlemode optical fiber that constitutes the sensor. The resultant increase in mass leads to a shift in their refractive indexes and thus the propagation constant of the fundamental mode. That shift can be detected as a phase shift in the light emerging from the fiber. Calculations that have been presented based on the certain idealizations are very encouraging. However, the response of the sensor should be calculated under realistic conditions, which can be simulated by the Los Alamos MCNP code. One sensor design has been presented, and issues such as radiation-induced darkening and the production of unstable isotopes have been briefly discussed.

Acknowledgments

The author thanks J.S. Accetta, CEO of JSA Photonics, and P.E Bolduc and B. P. Roth, both of Albuquerque, New Mexico, for their suggestions which led to improvements in the paper. The work was self-funded.

References

[1] G. Rajan, J. Izewska, in: E. Podgorsak (Ed.), Radiation Oncology Physics: A Handbook for Teachers and Students, IAEA, Vienna, 2005, pp. 101–112 Available from: 〈http://www-naweb.iaea.org/NAHU/DMRP/documents/slides/Ch_04_MacForm.pdf〉.

[2] Neutron Monitor. Available from: 〈http://en.wikipedia.org/wiki/Neutron_monitor〉.
[3] Neutron Monitoring Instrumentation, GE Measurement and Control. Available from: 〈http://www.ge-mcs.com/en/nuclear-reactor-instrumentation/neutron-monitoring-instrumentation.html〉.
[4] J.S. Accetta, J.D. Weiss, Laser Focus World 1 (2010), Available from: 〈http://www.laserfocusworld.com/articles/2010/01/fiber-based-sensing-optical-fibers tackle-weapons-of-mass-destruction.html〉.
[5] Z.W. Bell, et al., Physica Status Solidi (c) 2 (2005) 1592 Available from 〈http://www1.y12.doe.gov/search/library/documents/pdf/ydz-2565.pdf〉.
[6] Information on Saint Gobain's scintillating optical fibers. Available from: 〈http://www.detectors.saint-gobain.com/uploadedFiles/SGdetectors/Documents/Brochures/Scintillating-Optical-Fibers-Brochure.pdf〉.
[7] F. Franceschini, F. Ruddy. in: R. Gerhardt (Ed.), Properties and Applications of Silicon Carbide, InTech, Croatia, 2011, pp. 275–296. Available from: 〈http://cdn.intechweb.org/pdfs/15095.pdf〉.
[8] Information on Corning singlemode fibers. Available from: 〈http://www.corning.com/WorkArea/showcontent.aspx?id=41261〉.
[9] A. Snyder, J. Love, Optical Waveguide Theory, Chapman and Hall, London and New York, 1983.
[10] D. Marcuse, Light Transmission Optics, second ed., Van Nostrand Reinhold Company, New York, 1982.
[11] B. Jeunhomme, Single-Mode Fiber Optics, second ed., Marcel Dekker, Inc., New York and Basel, 1990.
[12] The Corning Cutoff Wavelength Measurement Method. Available from: 〈http://www.corning.com/docs/opticalfiber/mm15_08-01.pdf〉.
[13] R.A. Sammut, Electronics Letters 15 (1979) 590.
[14] H.D. Rudolph, E.G. Neumann, Nachrichtentechnische Zeitschrift 29 (1976) 328.
[15] D.L. Wood, J.W. Fleming, The Review of Scientific Instruments 53 (1982) 43.
[16] J.W. Fleming, Applied Optics 23 (1984) 4486.
[17] J.H. Simmons., K.S. Potter, Optical Materials, Academic Press, San Diego, 2000.
[18] Wikipedia articles on the isotopes of germanium, silicon, and oxygen (and references contained therein).
[19] J.H. Cole, C. Kirkendahl, A. Dandridge, G. Cogdell, T.G. Giallorenzi, Journal of the Washington Academy of Sciences 90–3 (2004) 40, Available from: 〈http://www.washacadsci.org/Journal/Journalarticles/V.90-3-James%20H.%20Cole,%20Clay%20Kirkendall,%20Anthony%20Dandridge,%20Gary%20Cogdell,%20and%20T.G.%20Giallorenzi,.pdf〉.
[20] The MCNP Code is available from: 〈https://laws.lanl.gov/vhosts/mcnp.lanl.gov/〉.
[21] National Nuclear Data Center: Evaluated Nuclear Data File. Available from: 〈http://www.nndc.bnl.gov/exfor/endf00.jsp〉.
[22] E. Friebele, M. Gingerich, Applied Optics 20 (1981) 3448.
[23] K. Toh, T. Shikama, S. Nagata, B. Tsuchiya, M. Yamauchi, T. Nishitani, Measurement Science & Technology 17 (2006) 955.
[24] H. Henschel, O. Kohn, H. Schmidt, IEEE Transactions on Nuclear Science NS 43 (1996) 1050.
[25] E. Dianov, E. Nikitin, L. Kornienko, A. Rybaltovsky, P. Chernov, Optical and Quantum Electronics 11 (1979) 467.
[26] D. Rozelle, R. Michal, Apparatus and method for isolated photobleaching fiber optic rotation sensor coils, (2001) U.S. Patent #6205265.
[27] A company called Polymicro Technologies has long made such fibers, which are available from: 〈www.polymicro.com/〉.
[28] A company called Fibercore makes a pure-silica-core, singlemode fiber. Available from: 〈www.fibercore.com/Products/SMSeries/tabid/89/agentType/View/PropertyID/260/Default.aspx〉.